BTEX Gas Sensor Based on Hematite Microrhombuses

Luís F da Silva, Ariadne Catto, Sandrine Bernardini, Tomas Fiorido, João V.N. de Palma, Waldir Avansi, Khalifa Aguir, Marc Bendahan

BTEX Gas Sensor Based on Hematite Microrhombuses

Luís F. da Silva,[†,] Ariadne C. Catto,[†,‡] Sandrine Bernardini,[§] Tomas Fiorido,[§] João V. N. de Palma,[†] Waldir Avansi Jr,[†] Khalifa Aguir[§] and Marc Bendahan[§]*

[†]Laboratory of Nanostructured Multifunctional Materials, Department of Physics, Federal University of São Carlos, 13565-905, São Carlos, SP, Brazil

[‡]Center for the Development of Functional Materials, Federal University of São Carlos, 13565-905, São Carlos, SP, Brazil

[§]Aix Marseille Univ, Université de Toulon, CNRS, IM2NP, Marseille, France

ABSTRACT

Over the past fifty years, gas sensors based on metal semiconducting oxides (MOXs) have drawn attention due to their performance in detecting of various gases. Thus, we report herein on a BTEX gas sensor based on hematite (α-Fe_2O_3) microrhombuses synthesized via the hydrothermal method. X-ray diffraction and X-ray absorption spectroscopy analyses indicated the presence of a pristine hematite phase after hydrothermal treatment. Electron microscopy analyses revealed that the hematite sample consists of single-crystals with a rhombus-like shape and an average size of 140 nm. Electrical measurements pointed out that hematite microrhombuses were sensitive towards sub-ppm BTEX levels, in which the minimum detected level was 3 ppb and long-term stability was for 1 month. The results presented here demonstrate the potential of hematite microrhombuses as a sensing material to manufacture BTEX gas sensor devices.

KEYWORDS: Fe_2O_3; hematite; gas sensor; BTEX; benzene, toluene, ethylbenzene; xylenes.

1. INTRODUCTION

The development in industrial and agricultural activities, mainly in developing countries, has resulted in the enhancement of harmful gases dumped into the atmosphere, such as CO, NO, NO_2, O_3, and Volatile Organic Compounds (VOCs).[1–6] The presence of these gases could cause adverse effects on the climate and human life. According to the World Health Organization (WHO), these chemical species may cause serious diseases (e.g. heart and lung diseases, stroke, cancer and acute respiratory infections) or in severe cases, death.[6–9] It has been estimated that air pollution has been responsible for the death of 7 million people worldwide every year.[6] Furthermore, approximately 80% of the urban population is exposed (indoor and outdoor) towards pollution levels that exceed the guidelines recommended by health organizations.[3,6,10] Note that adequate levels of air pollution would also provide a lower demand for hospital admissions (or care), since hospitalizations would decrease.[7] Therefore, the continuous and efficient monitoring of atmospheric gas pollutants is essential.

Among the dangerous gases, BTEX (Benzene, Toluene, Ethylbenzene, and the three Xylene isomers) gases belong to the aromatic VOCs group.[11–15] The main sources for BTEX emissions are indoor and outdoor, such as gas stations, fuel storage, road traffic, and also household products, such as paints, solvents, waxes, pesticides, among others.[11–14] Various investigations focused on BTEX gases due to their toxic, mutagenic, and/or carcinogenic effects.[8,12,16–18] According to the OSHA (Occupational Safety and Health Administration), permissible employee exposure to BTEX gases is an average concentration of 0.5 ppm (parts-per-million) for benzene, 200 ppm for toluene and 100 ppm for ethylbenzene and xylene.[12]

Generally, BTEX gases have been identified and quantified using gas chromatography.[11,17] However, this equipment, besides being expensive, is not portable,

making in-situ analyses difficult.[13] Thus, several investigations have focused on the development of portable devices that allow efficient detection and monitoring of BTEX gases in indoor and outdoor environments.

In past decades, MOXs have been widely used in resistive-type gas sensors to detect (non-) toxic gases. Their main advantages are the low cost, small size, high sensitivity and stability, fast response/recovery and portability.[4,19–21] MOXs have been widely used as sensing layers for detecting BTEX gases, such as WO_3, ZnO, MoO_3,[12,14,22,23] and also some heterojunctions, for example, SnO_2/V_2O_5, and CuO/SnO_2.[24,25]

Hematite (α-Fe_2O_3) is an n-type wide band-gap semiconductor (E_g = 2.1 eV, at 300 K).[26] It is the most abundant and the cheapest MOX obtained in the Earth'crust,[27] exhibiting potential applications in photocatalysis, energy generation, lithium batteries and the gas sensor area.[2,26–32] **The Fe_2O_3 compound has been studied as sensing layer for detection of a wide range of analytes.[33-38] For example, Tian and co-workers prepared hematite nanoboxes via metal-organic frameworks method. The authors observed such nanoboxes were highly sensitive to H_2S gas for an optimum temperature of 200°C, besides exhibiting a good selectivity towards NO, CO, and NH_3 gas.[38] Despite the remarkable gas-sensing properties of hematite, few researchers have paid attention to its performance for detecting BTEX gases. Kim co-workers prepared vertically hematite nanotubes applied as a gas-sensing layer. They observed a higher response towards acetone compared to other analytes (benzene, toluene, acetone, ethanol, and CO), for an operating temperature relatively high equal to 350°C.[27] Also, Thu and co-workers reported good selectivity and sensitivity to ethanol of a hematite nanoporous sample working at 400°C. In a similar work, Park and co-workers observed for**

hematite microcubes a high sensitivity to VOCs, especially formaldehyde, at an operating temperature of 300°C.[31]

Motivated by these arguments, we report herein a versatile and efficient approach to obtain hematite microcrystals presenting remarkable properties for application as a BTEX gas-sensing layer. The microcrystals were synthesized via the hydrothermal method and characterized by using X-ray diffraction (XRD), field-emission scanning electron (FE-SEM) and high-resolution transmission electron microscopies (HR-TEM), and X-ray absorption near-edge structure (XANES) spectroscopy. The α-Fe_2O_3 microcrystals were studied in the detection of BTEX, acetone, and ethanol. Electrical measurements revealed their higher sensitivity to sub-ppb BTEX levels compared to other VOCs. These results have a significant impact on the scientific field due to its practical potential for environmental monitoring applications.

2. EXPERIMENTAL SECTION

2.1. Preparation of microcrystals

The α-Fe_2O_3 microcrystals were obtained by the hydrolysis of iron (III) chloride hexahydrate ($FeCl_3.6H_2O$, 99.9%, Sigma-Aldrich) in ethyl alcohol anhydrous at room temperature. The concentration of iron chloride diluted in alcohol was 0.06 M. Afterwards, deionized water was slowly added to the reactional solution to obtain a molar ratio of Fe(III) : H_2O = 1:500. The chloride anions were removed by the dialysis process, and the precipitate was then dried in an electric oven during 12 h at 80°C. To obtain the hematite phase, the precipitate powder was diluted in deionized water (1 g. L^{-1}) and then submitted to hydrothermal treatment for 4 hours at 200°C with a heating rate of 2°C min^{-1}. The precipitated powders were washed with deionized water and isopropyl alcohol and dried at 80°C overnight under the air atmosphere.

2.2. Characterization Techniques

X-ray diffraction (XRD) measurements were carried out using CuKα radiation (Rigaku diffractometer, model D/Max-2500PC) in a 2θ range from 20° to 80° with a step of 0.02° at a scanning speed of 2° min^{-1}. The morphological properties were investigated using a field emission scanning electron microscopy (FE-SEM, Zeiss Supra35) and a transmission electron microscopy (TEM, FEI Tecnai G2 F20) operated at 200 KeV, respectively. The mean particle size was estimated by analyzing FE-SEM micrographs through the measure of approximately 100 particles. X-ray absorption spectroscopy (XAS) experiments were carried out at the D08B-XAFS2 beamline on the Brazilian Synchrotron Light Laboratory (LNLS). The experiments were carried out at the Fe K-edge (7112 eV) in a transmission mode at room temperature using a flat Si(111) double crystal monochromator. X-ray Absorption Near-Edge Structure (XANES) spectra were collected for each sample between 7090 and 7190 eV using energy steps of 0.5 eV. For the sake of comparison, all spectra were background removed and normalized using as unity the first EXAFS (Extended X-ray Absorption Fine Structure) oscillation using MAX software.[39]

2.3. Gas-sensing Experiments

Hematite microcrystals were dispersed in isopropyl alcohol (20 mg mL^{-1}) using an ultrasonic cleaner for 30 min and then the suspension was dropped three times onto a Si/SiO_2 substrate containing 100 nm thick Pt interdigitated electrodes separated by a distance of 50 μm. After deposition, the sensor was then treated at 500°C in an electric oven under the air atmosphere for 1 h at a heating rate of 10°C min^{-1}. The photography of the sensing platform and FE-SEM images of the hematite microcrystals used in the experiments are presented in Fig.1.

Insert Figure 1

Gas-sensing experiments were carried out in a dynamic chamber that allows us to control the operating temperature and to obtain various gas concentrations by using Mass Flow Controllers (MFC).[12] This workbench, Fig.2, can produce low BTEX concentrations from 1 to 400 ppb (part-per-billion) **from the dilution with dry air. The total gas flow rate was kept constant and equal to 500 SCCM. The workbench also allows the control of relative humidity (% RH) from 0 to 90%. The cylinder with the BTEX gases mixture was purchased from Air Liquide company (France). The concentration of each component in the BTEX mixture is displayed in Table S1.** Further details regarding the gas-sensing workbench may be found in previous work in Ref. 12. The applied DC voltage was kept constant, while the electrical resistance was monitored using a sourcemeter (Keithley, model 2540). The sensor response (S) was defined as $S(\%) = ((R_{air} - R_{BTEX})/R_{air}).100$, where R_{air} and R_{BTEX} are the electrical resistances of the sensor upon exposure to dry air and BTEX gases, respectively. **The response time was defined as the time required for the electrical resistance to reach 90% of the initial value when exposed to the BTEX gases. Similarly, the recovery time was defined as the time required for the electrical resistance to recover 90% of the initial value after switching off the BTEX gas flow.**

Insert Figure 2

3. RESULTS AND DISCUSSION

3.1. Microstructural Properties

X-ray diffraction pattern of the as-synthesized sample prepared via the hydrothermal route is shown in Fig.S1(a). All reflections were indexed to a pristine rhombohedral hematite (α-Fe_2O_3)

phase with an R3c space group (JCPDS file 87-1164). Fe K-edge spectra of iron-oxide based compounds and the as-prepared hematite sample are displayed in Fig.3(a)-(b). The comparison of reference compound spectra with the sample confirms the presence of the pristine α-Fe_2O_3 phase, with iron atoms in octahedral coordination, FeO_6.[30]

FE-SEM image in Fig.3(c) reveals a homogeneity of the morphology of the as-studied microcrystals that exhibit a well-defined rhombus-like shape with an average size of approximately 140 nm. The HRTEM image of a selected region of an individual crystal and their respective Fourier Transform (FT), Fig.3(d), shows the monocrystalline nature of the as-studied sample.

Insert Figure 3

3.2. BTEX Sensing Performances

Gas-sensing performances of α-Fe_2O_3 microrhombuses were evaluated towards BTEX gases. Initially, the optimum operating temperature of the sample was evaluated by exposing it to 100 ppb of the analyte and varying only the operating temperature, as seen in Fig.4. The electrical measurements carried out at different working temperatures are presented in Fig.S2. For temperatures below 200°C, no sensitivity towards BTEX gases was observed.

The highest sample responses were achieved in the temperature range of 240 to 280°C, as shown in Fig.4**(a). In addition, the behavior of response and recovery times as a function of operating temperature is displayed in Fig.4(b). We can observe that despite the sample required a long time for the complete desorption of BTEX molecules, its response time was relatively fast at around 50 s. To assert the high sensitivity of the microrhombuses, they were**

then exposed to 100 ppb of BTEX during different time intervals (from 5 s to 360 s), as shown in Fig.4(c). The sample was sensitive to various exposure times to BTEX gases, mainly, for the shorter time, i.e., 5 s. Moreover, the sample saturation level was reached at exposure times longer than 180 s, as illustrated in the inset of Fig.4(c). It is interesting to note that, even after a long sequence of exposure cycles (> 8 h) the sample exhibited a total recovery, indicating that its surface was not damaged.

To obtain short recovery times of the sensing material, we chose 280°C as the optimum working temperature for further experiments.

Insert Figure 4

The hematite microrhombuses were kept at 280°C and then exposed to several different BTEX levels, from 3 till 400 ppb. It should be mentioned that for gas levels lower than 3 ppb, the microcrystals did not exhibit any sensitivity; considering here the abovementioned temperature.

Fig.5 shows that the electrical resistance of the microrhombuses decreased during exposition to BTEX gases. When an n-type MOX, such as hematite, is exposed to a reducing gas (e.g. BTEX) the ionized oxygen anions adsorbed at the surface sample oxidize the analyte. During this adsorption process, the release of the electrons occurs from the MOX surface, consequently decreasing the electrical resistance of the sensing material.[5,35,40,41]

Regarding the sensor responses, the hematite microcrystals showed good sensitivity even for very low BTEX levels, in addition to complete recovery after each exposure cycle. Furthermore, the sample also exhibited high repeatability of its response, reinforcing its reliability, as demonstrated by the seven exposure cycles displayed in Fig.5(d).

Insert Figure 5

Fig.6 displays the sensor response of α-Fe_2O_3 microrhombuses, kept at 280°C, exposed towards different BTEX levels, from 3 to 400 ppb. The response enhancement as a function of the BTEX level is clear, with no evidence of saturation in the evaluated range. Despite the fact that the microcrystals had detected sub-ppm gas levels, the inset of Fig.6 shows that the response has a low variation between 3 and 10 ppb, meaning a low accuracy in this range. Nevertheless, this finding does not debunk the hematite for practical applications, as long as just BTEX levels above 500 ppb become harmful to human health, as recommended by the WHO.

Regarding the sensor response behaviors with BTEX levels, an exponential trend in the sensor response of hematite microrhombuses was obtained. It is well established that the sensor response (S) of MOXs complies with the following power-law equation: $S(C) = A(C)^n$, where A is a constant, *n* the exponent, and *C* is the concentration of the investigated analyte.[42] Herein, the best fitting law acquired from the experimental data was found to be the equation: $S(C)= 7{,}617.(C)^{0,461}$, respectively.

Insert Figure 6

The influence of relative humidity on the BTEX gas sensing performance was also investigated. For that, the sample was kept at 280 °C and then exposed towards 100, 200, 300, and 400 ppb of BTEX gases under different relative humidity (0, 20, and 40 % RH) values. It can be seen that the BTEX sensor response was affected by the presence of water molecules, as shown in Fig.7. This behavior is due to the competition of water and BTEX molecules by actives sites on the sample's surface, this reducing its sensing performance towards BTEX gases. Zhang and co-workers reported similar effect of the humidity for WO_3

nanosheets used as sensing material to BTEX (Benzene, Toluene, Ethylbenzene, and p-Xylol) vapors.[14]

Insert Figure 7

Gas selectivity and long-term stability are desirable characteristics in the development of gas sensor devices. **Fig. 8(a)** illustrates the response (S) of the microrhombuses, at 280°C, exposed to BTEX gases, ethanol, and acetone gases. Notably, the hematite microrhombuses exhibited a higher response to BTEX gases compared to the investigated VOCs gases. Regarding the long-term stability, it was evaluated by exposing the microrhombuses towards 100 ppb of BTEX gases for 30 days, and the results are presented in **Fig. 8(b)**. It can be noted after the mentioned period that the sample still detected a very low BTEX level. It means that the lifetime of the hematite microrhombuses can be superior to 1 month since the sample surface was not poisoned/damaged due to the several exposures to BTEX gases.

Insert Figure 8

Table 1 shows the performance of some MOXs synthesized by different methodologies, applied as a BTEX gas sensing material. As seen, the range of working temperatures of such MOXs is similar to those found here for the microrhombuses. Nevertheless, we must draw attention to the sensitivity of hematite microrhombus that detected a very low BTEX level, i.e., 3 ppb. Based on the findings presented here, it is reasonable to consider the potential of hematite microcrystals as a sensing material for BTEX sensors.

Table 1. Gas-sensing performance of the MOXs used as a BTEX sensing material.

Sensing material	Processing method	$T_{opt.}$ (°C)	BTEX level* (ppb)	Reference
m-WO_3	RF-sputtering	260	5	12
h-WO_3	Hydrothermal	320	1000	14
Au-ZnO	Hydrothermal	206	1000	43
Au-MoO_3	Solvothermal	250	100	23
CuO/SnO_2	Microwave-assisted	280	2000	24
SnO_2/V_2O_5	Sol-gel	270	500	25
α-Fe_2O_3	Hydrothermal	240-280	3	Our work

*Minimum BTEX level, experimentally, detected.

3.3. Gas-Sensing Mechanism

We propose herein a possible sensing mechanism of the hematite microrhombuses to detect BTEX, i.e., Benzene (C_6H_6), Toluene ($C_6H_5CH_3$), Ethylbenzene (C_8H_{10}) and Xylene ($C_6H_4(CH_3)_2$) gases. According to the literature, for resistive-type gas sensors, the sensing mechanism is based on the adsorption process of the oxygens and the target gas molecules which occurs on the MOX surface, depending on the sensing material characteristics (e.g. particles size, and morphology), working temperature, analyte concentration, environment conditions (e.g. pressure, and humidity), etc.[41,44-48]

Regarding the hematite microrhombuses, when the oxygen molecules are adsorbed on the sample surface, they trap free electrons from the hematite conduction band. This ionosorption process increases the band bending (qV_s), forming a depletion region "*d*" on the hematite microrhombuses surface, as illustrated in **Fig.9(a)-(b)**. At operating temperatures higher than 280°C, the ionic O^- species are dominant.[5,13,46] This process can be expressed by:

$$O_{2(ads)} + 2e^- \rightarrow 2O^-_{(ads)} \quad (1)$$

Upon exposure to a reducing gas, such as BTEX gases, the electrical resistance of the hematite decreases due to the reaction between the molecules of the reducing gas and the ionosorberd oxygens (O^-) at the rhombus surface, releasing the electrons to the conduction band. This behavior reduces the height of potential barrier qV_s, consequently decreasing the depletion region "*d*" and enhancing the conductivity of the hematite microrhombuses.[44,45,49] **Fig. 9(b)** illustrates the possible sensing mechanism of hematite microrhombuses to detect BTEX gases. In this figure, it is suggested that the possible sub-products formed by the interaction between the BTEX gases and sample surface are H_2O and CO_2.

Insert Figure 9

CONCLUSION

In summary, we report here the synthesis of hematite microcrystals via hydrothermal route for use as BTEX gases-sensing material. XRD pattern and Fe K-edge XANES spectra revealed the presence of the pristine hematite phase. FE-SEM and HR-TEM analyses showed that hematite microcrystals exhibit a well-defined rhombus-like shape with a single-crystal nature. Electrical measurements showed a good sensitivity towards BTEX gases at an operating temperature of 280°C. The microrhombuses detected the lowest gas levels that ranged from 3 ppb to 400 ppb, exhibiting excellent repeatability and stability, and good selectivity towards acetone and ethanol. Finally, the findings presented here highlighted the promising properties of hematite microrhombuses as BTEX gas sensors for practical applications.

Corresponding Author

*E-mail: lfsilva83@gmail.com.

Author Contributions

The manuscript was written through contributions of all authors. All authors have given approval to the final version of the manuscript.

ACKNOWLEDGMENT

The authors thank Dr. Julio C. Sczancoski for the XRD data and Mr. Rorivaldo Camargo who operated the FE-SEM microscope. This investigation was initiated in the Institute of Material and Microelectronics of Provence in France during a period of visiting professor at the Aix-Marseille University. This research was also partially performed at the Brazilian Nanotechnology National Laboratory (Microfabrication team: Project LMF-18580), and the Brazilian Laboratory of

Synchrotron Radiation (LNLS, Project D04B-XAFS2-20180311), Campinas, SP, Brazil. We also thank the Laboratory of Structural Characterization (LCE/DEMa/UFSCar) for the TEM facilities. The authors acknowledge the financial support of the Brazilian research funding institution FAPESP (under grants No. 2017/12437-5, 2019/18082-2, 2018/18208-0 and 2013/07296-2), CNPq (under grants No. 405140/2018-5, 426511/2018-2, 308706/2018-8, and 311463/2017-7) and CAPES.

REFERENCES

[1] P.M. Lemieux, C.C. Lutes, D.A. Santoianni, Emissions of organic air toxics from open burning: A comprehensive review, Prog. Energy Combust. Sci. 30 (2004) 1–32.

[2] A. Mirzaei, B. Hashemi, K. Janghorban, α-Fe_2O_3 based nanomaterials as gas sensors, J. Mater. Sci. Mater. Electron. 27 (2016) 3109–3144.

[3] A.C. Catto, L.F. da Silva, M.I.B. Bernardi, S. Bernardini, K. Aguir, E. Longo, V.R. Mastelaro, Local structure and surface properties of $Co_xZn_{1-x}O$ thin films for ozone gas sensing, ACS Appl. Mater. Interfaces 8 (2016) 26066–26072.

[4] W. Avansi Jr, A.C. Catto, L.F. da Silva, T. Fiorido, S. Bernardini, V.R. Mastelaro, K. Aguir, R. Arenal, One-dimensional V_2O_5/TiO_2 heterostructures for chemiresistive ozone sensors, ACS Appl. Nano Mater. 2, (2019) 4756–4764.

[5] H.-J. Kim, J.-H. Lee, Highly sensitive and selective gas sensors using p-type oxide semiconductors: Overview, Sens. Actuators, B 192 (2014) 607–627.

[6] World Health Organization - WHO/Health Topics/ Air Pollution, https://www.who.int/health-topics/air-pollution#tab=tab_1, (accessed in 28 February 2020).

[7] C.K. Abe, G.S. Miraglia, Health impact assessment of air pollution in São Paulo, Brazil, Int. J. Environ. Res. Public Heal. 13 (2016) E694.

[8] M. Kampa, E. Castanas, Human health effects of air pollution, Environ. Pollut., 151 (2008) 362–367.

[9] S.-Y. Lin, S.-W. Ju, C.L. Lin, W.-H. Hsu, C.-C. Lin, I.-W. Ting, C.-H. Kao, Air pollutants and subsequent risk of chronic kidney disease and end-stage renal disease: A population-based cohort study, Environ. Pollut. 261 (2020) 114154.

[10] S. Saksena, P.B. Singh, R.K. Prasad, R. Prasad, P. Malhotra, V. Joshi, R.S. Patil, Exposure of infants to outdoor and indoor air pollution in low-income urban areas - A case study of Delhi, J. Expo. Sci. Environ. Epidemiol. 13 (2003) 219-230.

[11] I. Lara-lbeas, A. Rodríguez-Cuevas, C. Andrikopoulou, V. Person, L. Baldas, S. Colin, S. Le Calvé, Sub-ppb level detection of BTEX gaseous mixtures with a compact prototype GC equipped with a preconcentration unit, Micromachines, 2019, 10, 187.

[12] A. Favard, K. Aguir, T. Contaret, A. Dumas, M. Bendahan, Detection and measuring of BTEX traces at the ppb level using metal oxide gas sensor, Mater. Today Proc., 6 (2019) 323–327.

[13] A. Mirzaei, J.-H. Kim, H.W. Kim, S.S. Kim, Resistive-based gas sensors for detection of benzene, toluene and xylene (BTX) gases: A Review, J. Mater. Chem. C 6 (2018) 4342–4370.

[14] D. Zhang, Y. Fan, G. Li, Z. Ma, X. Wang, Z. Cheng, J. Xu, Highly sensitive BTEX sensors based on hexagonal WO_3 nanosheets, Sens. Actuators, B 293 (2019) 23–30.

[15] A. Allouch, S. Le Calvé, C.A. Serra, Portable, miniature, fast and high sensitive real-time analyzers: BTEX detection, Sens. Actuators, B 182 (2013) 446–452.

[16] R. Duarte-Davidson, C. Courage, L. Rushton, L. Levy, Benzene in the environment: An assessment of the potential risks to the health of the population, Occup. Environ. Med., 58 (2001) 2-13.

[17] A. Rafiee, J.M. Delgado-Saborit, P.D. Sly, H. Amiri, M. Hoseini, Lifestyle and occupational factors affecting exposure to BTEX in municipal solid waste composting facility workers, Sci. Total Environ., 656 (2019) 540–546.

[18] S.M. Correa, G. Arbilla, M.R.C. Marques, K.M.P.G. Oliveira, The impact of BTEX emissions from gas stations into the atmosphere, Atmos. Pollut. Res., 3 (2012), 163–169.

[19] N. Barsan, D. Koziej, U. Weimar, Metal oxide-based gas sensor research: How to?, Sens. Actuators, B 121 (2007) 18–35.

[20] L.F. da Silva, A.C. Catto, W. Avansi Jr, L.S. Cavalcante, J. Andres, K. Aguir, V.R. Mastelaro, E. Longo, A novel ozone gas sensor based on one-dimensional (1D) α-Ag_2WO_4 nanostructures, Nanoscale 6 (2014) 4058–4062.

[21] L.F. da Silva, J.-C. M'Peko, A.C. Catto, S. Bernardini, V.R. Mastelaro, K. Aguir, C. Ribeiro, E. Longo, UV-enhanced ozone gas sensing response of ZnO-SnO_2 heterojunctions at room-temperature, Sens. Actuators, B 240 (2017) 573–579.

[22] S.P. Choudhury, Z. Feng, C. Gao, X. Ma, J. Zhan, F. Jia, BN quantum dots decorated ZnO nanoplates sensor for enhanced detection of BTEX gases, J. Alloys Compd. 815 (2020) 152376.

[23] L. Sui, X. Zhang, X. Cheng, P. Wang, Y. Xu, S. Gao, H. Zhao, L. Huo, Au-loaded hierarchical MoO_3 hollow spheres with enhanced gas-sensing performance for the detection of BTX (benzene, toluene, and xylene) and the sensing mechanism, ACS Appl. Mater. Interfaces 9 (2017) 1661–1670.

[24] F. Ren, L. Gao, Y. Yuan, Y. Zhang, A. Alqrni, O.M. Al-Dossary, J. Xu, Enhanced BTEX gas-sensing performance of CuO/SnO_2 composite, Sens. Actuators, B 223 (2016) 914–920.

[25] F. Zhang, X. Wang, J. Dong, N. Qin, J. Xu, Selective BTEX sensor based on a SnO_2/V_2O_5 composite, Sens. Actuators, B 186 (2013) 126–131.

[26] G. Bailly, J. Rossignol, B. de Fonseca, P. Pribetich, D. Stuerga, Microwave gas sensing with hematite: Shape effect on ammonia detection using pseudocubic, rhombohedral, and spindlelike particles, ACS Sensors 1 (2016) 656–662.

[27] D.H. Kim, Y.-S. Shim, J.-M. Jeon, H.Y. Jeong, S.S. Park, Y.-W. Kim, J.-S. Kim, J.-H. Lee, H.W. Jang, Vertically ordered hematite nanotube array as an ultrasensitive and rapid response Acetone Sensor, ACS Appl. Mater. Interfaces, 6 (2014) 14779–14784.

[28] N.D. Cuong, T.T. Hoa, D.Q. Khieu, N.D. Hoa, N. Van Hieu, Gas sensor based on nanoporous hematite nanoparticles: Effect of synthesis pathways on morphology and gas sensing properties, Curr. Appl. Phys., 12 (2012) 1355–1360.

[29] J. García-Serrano, E. Gómez-Hernández, M. Ocampo-Fernández, U. Pal, Effect of Ag doping on the crystallization and phase transition of TiO_2 nanoparticles, Curr. Appl. Phys., 9 (2009) 1097–1105.

[30] C. Wu, P. Yin, X. Zhu, C. OuYang, Y. Xie, Synthesis of hematite (α-Fe_2O_3) nanorods: Diameter-size and shape effects on their applications in magnetism, lithium ion battery, and gas sensors, J. Phys. Chem. B 110 (2006) 17806–17812.

[31] H.J. Park, S.Y. Hong, D.H. Chun, S.W. Kang, J.C. Park, D.-S. Lee, A highly susceptive mesoporous hematite microcube architecture for sustainable p-type formaldehyde gas sensors, Sens. Actuators, B 287 (2019) 437–444.

[32] T. Ma, L. Zheng, Y. Zhao, Y. Xu, J. Zhang, X. Liu, Highly porous double-shelled hollow hematite nanoparticles for gas sensing, ACS Appl. Nano Mater., 2 (2019) 2347–2357.

[33] M. Debliquy, C.Baroni, A. Boudiba, J.-M.Tulliani, M. Olivier, C. Zhang., Sensing characteristics of hematite and barium oxide doped hematite films towards ozone and nitrogen dioxide, Procedia Eng. 25 (2011) 219-222.

[34] Z. Wu, Z. Li, H. Li, M. Sun, S. Han, C. Cai, W. Shen, Y. Fu, Ultrafast response/recovery and high selectivity of the H_2S gas sensor based on α-Fe_2O_3 nano-ellipsoids from one-step hydrothermal synthesis, ACS Appl. Mater. Interf. 11 (2019)

12761-12769.

[35] D. Peeters, D. Barreca, G. Carraro, E. Comini, A. Gasparotto, C. Maccato, C. Sada, G. Sberveglieri, Au/ε-Fe_2O_3 nanocomposites as selective NO_2 gas sensors, J. Phys. Chem. C 118 (2014) 11813–11819.

[36] V. Balouria, A. Kumar, S. Samanta, A. Singh, A.K. Debnath, A. Mahajan, R. K. Bedi, D.K. Aswal, S.K. Gupta, Nano-crystalline Fe_2O_3 thin films for ppm level detection of H_2S, Sens. Actuators, B 181 (2013) 471-478.

[37] V.V Malyshev, A.V. Eryshkin, E.A. Koltypin, E.A. Varfolomeev, A.A. Vasiliev, Gas sensitivity of semiconductor Fe_2O_3-based thick-film sensors to CH_4, H_2, NH_3, Sens. Actuators, B 19 (1994) 434-436.

[38] K. Tian, X.X. Wang, Z.Y. Yu, H.Y. Li, X. Guo, Hierarchical and hollow Fe_2O_3 nanoboxes derived from metal–organic frameworks with excellent sensitivity to H_2S, ACS Appl. Mater. Interf. 9 (2017) 29669-29676.

[39] A. Michalowicz, J. Moscovici, D. Muller-Bouvet, K. Provost, MAX: Multiplatform Applications for XAFS, J. Phys. Conf. Ser., 190 (2009) 12034.

[40] D. Flak, A. Braun, B.S. Mun, J.B. Park, M. Parlinska-Wojtan, T. Graule, M. Rekas, Spectroscopic assessment of the role of hydrogen in surface defects, in the electronic structure and transport properties of TiO_2, ZnO and SnO_2 nanoparticles, Phys. Chem. Chem. Phys., 15 (2013) 1417–1430.

[41] C. Malagù, A. Giberti, S. Morandi, C.M. Aldao, Electrical and spectroscopic analysis in nanostructured SnO_2: 'Long-term' resistance drift is due to in-diffusion, J. Appl. Phys., 110 (2011) 93711.

[42] G. Lu, J. Xu, J. Sun, Y. Yu, Y. Zhang, F. Liu, UV-enhanced room temperature NO_2 sensor using ZnO nanorods modified with SnO_2 nanoparticles, Sens. Actuators, B 162 (2012) 82–88.

[43] Z. Shen, X. Zhang, X. Ma, R. Mi, Y. Chen, S. Ruan, The significant improvement for BTX (benzene, toluene and xylene) sensing performance based on Au-decorated hierarchical ZnO porous rose-like architectures, Sens. Actuators, B 262 (2018) 86–94.

[44] K. Suematsu, K. Watanabe, M. Yuasa, T. Kida, K. Shimanoe, Effect of ambient oxygen partial pressure on the hydrogen response of SnO_2 semiconductor gas sensors, J. Electrochem. Soc. 166 (2019) 618-622.

[45] M. Hübner, C.E. Simion, A. Tomescu-Stănoiu, S. Pokhrel, N. Bârsan, U. Weimar, Influence of humidity on CO sensing with p-type CuO thick film gas sensors, Sens. Actuators, B 153 (2011) 347–353.

[46] N. Bârsan, U. Weimar, Understanding the fundamental principles of metal oxide based gas sensors; The example of CO sensing with SnO_2 sensors in the presence of humidity, J. Phys. Condens. Matter. 15 (2003) R813.

[47] G. Korotcenkov, B.K. Cho, Spray pyrolysis deposition of undoped SnO_2 and In_2O_3 films and their structural properties, Prog. Cryst. Growth Charact. Mater. 63 (2017) 1–47.

[48] D.R. Miller, S.A. Akbar, P.A. Morris, Nanoscale metal oxide-based heterojunctions for gas sensing: A Review, Sens. Actuators, B 204 (2014) 250–272.

[49] A. Gurlo, N. Bârsan, A. Oprea, M. Sahm, T. Sahm, U. Weimar, An n- to p-type conductivity transition induced by oxygen adsorption on α-Fe_2O_3, Appl. Phys. Lett. 85 (2004) 2280–2282.

Title of Figures

Figure 1. (a) Photography of sensing platform based on hematite microcrystals compared to a U.S quarter-dollar coin. (b)-(c) FE-SEM images show the homogeneity of the thick film.

Figure 2. Experimental workbench used in the gas-sensing experiments of BTEX gases.

Figure 3. The as-prepared α-Fe_2O_3 microcrystals prepared via hydrothermal treatment. (a) Fe K-edge XANES spectra. (b) Details of the pre-edge XANES region. For the sake of comparison, the iron oxide reference compounds (FeO, α-Fe_2O_3, γ-Fe_2O_3 and Fe_3O_4) were added. (c) FE-SEM and (d) HR-TEM micrographs. The respective Fourier Transform (FT) of HRTEM images is presented in the inset of Fig.3(d).

Figure 4. (a) Gas-sensing performance of α-Fe_2O_3 microrhombuses, exposed towards 100 ppb of BTEX gases, and (b) variation of response and recovery times, at operating temperatures between 200 and 280°C. (c) Electrical resistance of the microrhombuses exposed during different time intervals to BTEX gases. The inset shows the evolution of sensor response with exposure time.

Figure 5. Gas-sensing response of the α-Fe_2O_3 microrhombuses kept at 280°C and exposed to different BTEX levels: (a) 3 to 10 ppb, (b) 10 to 30 ppb and (c) 100 to 400 ppb. (d) Sensor response for seven exposure cycles of 100 ppb of BTEX gases.

Figure 6. Sensor response of the α-Fe_2O_3 microrhombuses *vs*. BTEX level. The inset shows the response variation for a BTEX level between 3 and 10 ppb.

Figure 7. Sensor response of the α-Fe_2O_3 microrhombuses *vs*. BTEX level under different relative humidity (% RH) values, at an operating temperature of 280 °C.

Figure 8. Sensor performance of α-Fe_2O_3 microrhombuses at 280ºC. (a) Comparison of the response for an exposure of 0.1 ppm of BTEX gases, 100 ppm of acetone, and 100 ppm of ethanol. (b) Response of the sample upon exposure to 100 ppb of BTEX gases for 30 days.

Figure 9. Schematic illustration of the sensing mechanism of hematite rhombus-like crystals to detect BTEX gases. (a) Under air atmosphere, and (b) exposure to BTEX gases.

FIGURES

Fig.1

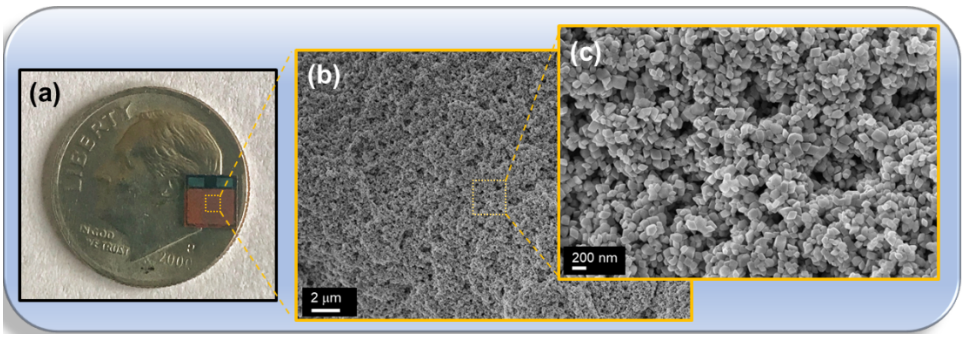

Fig.2

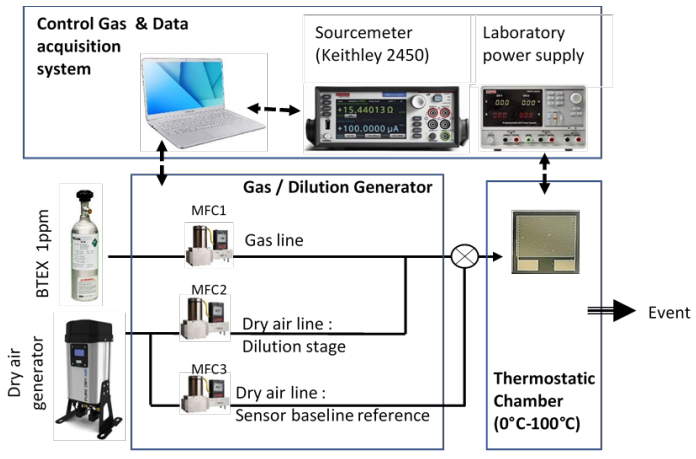

Fig3

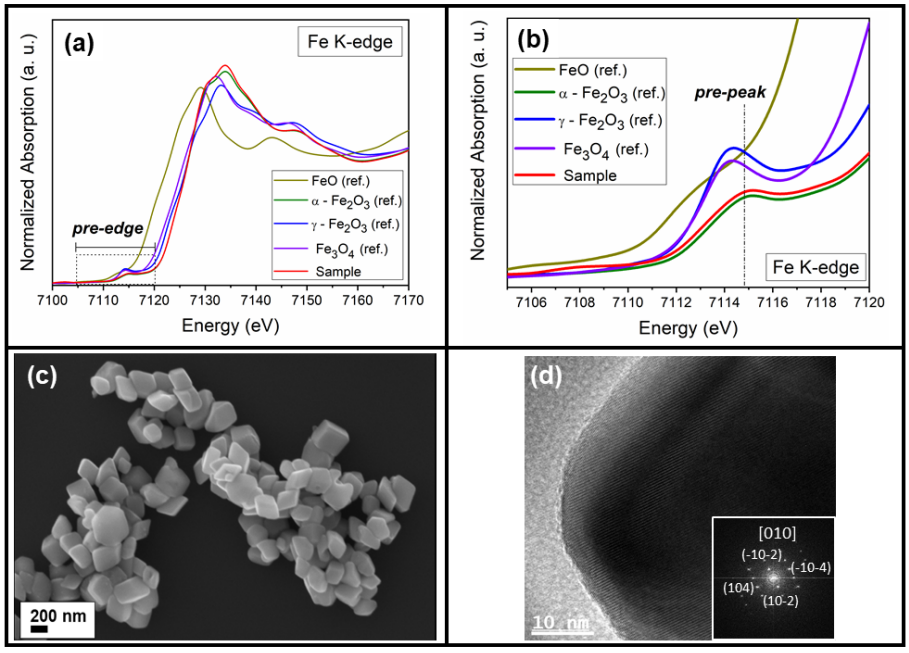
(a)
Fe K-edge
pre-edge
FeO (ref.)
α - Fe2O3 (ref.)
γ - Fe2O3 (ref.)
Fe3O4 (ref.)
Sample
Normalized Absorption (a. u.)
Energy (eV)
(b)
pre-peak
Fe K-edge
(c)
200 nm
(d)
[010]
(-10-2)
(-10-4)
(104)
(10-2)
10 nm

Fig4

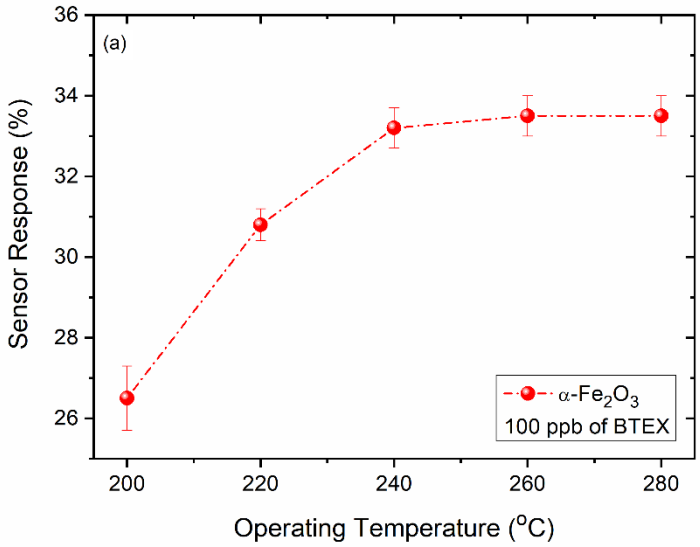
(a)
Sensor Response (%)
Operating Temperature (°C)
α-Fe2O3
100 ppb of BTEX

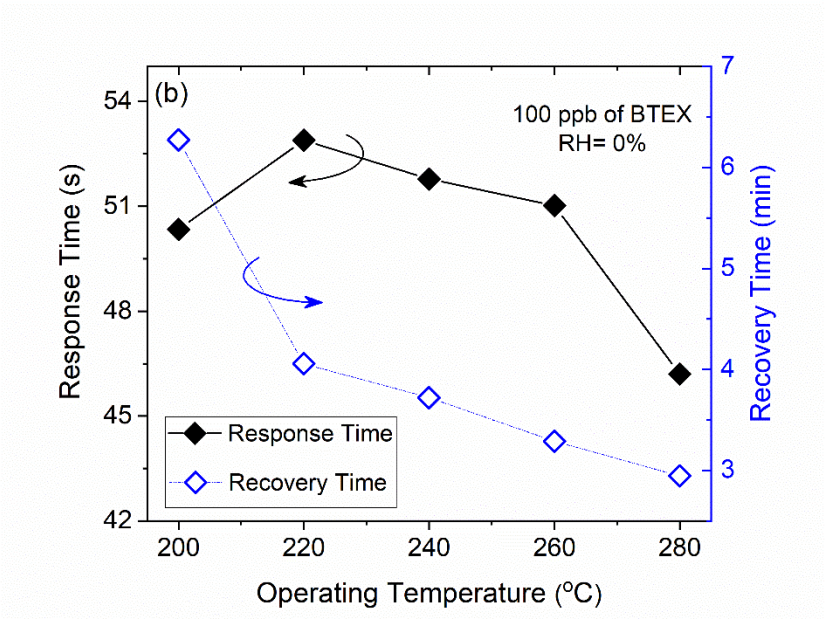
(b)
100 ppb of BTEX
RH= 0%
Response Time (s)
Recovery Time (min)
Operating Temperature (°C)
Response Time
Recovery Time

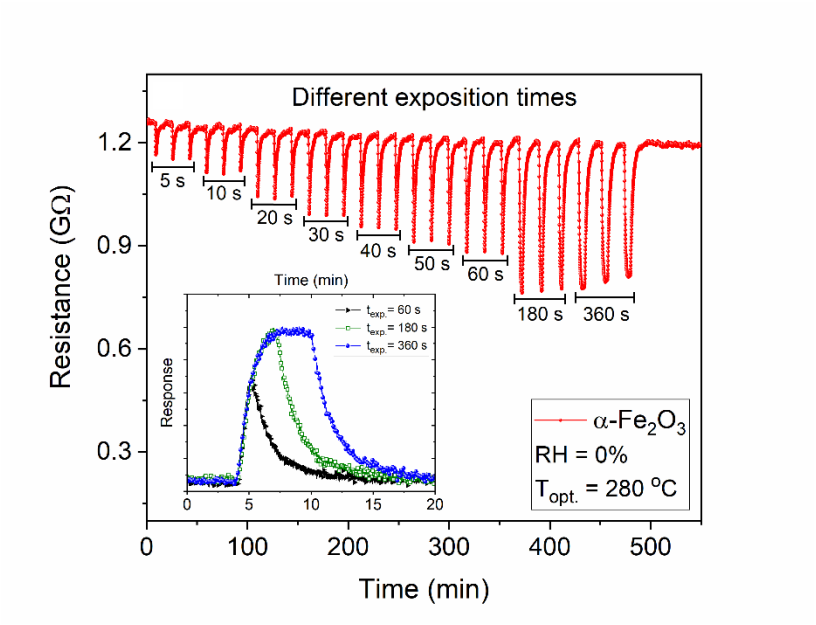
Different exposition times
Resistance (GΩ)
Time (min)
5 s
10 s
20 s
30 s
40 s
50 s
60 s
180 s
360 s
Response
$t_{exp.}$ = 60 s
$t_{exp.}$ = 180 s
$t_{exp.}$ = 360 s
α-Fe_2O_3
RH = 0%
$T_{opt.}$ = 280 °C

Fig.5

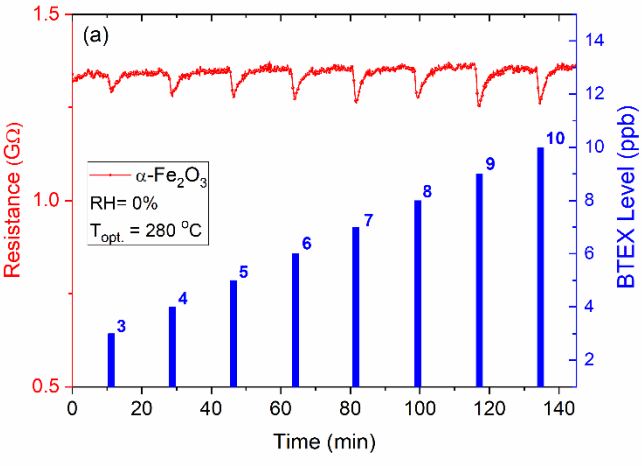
(a)
Resistance (GΩ)
BTEX Level (ppb)
Time (min)
α-Fe_2O_3
RH= 0%
$T_{opt.}$ = 280 °C
3
4
5
6
7
8
9
10

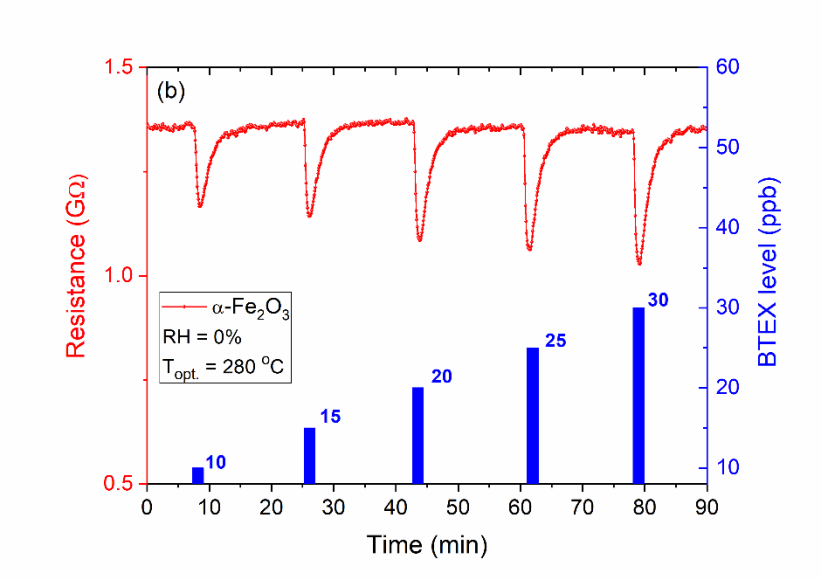
(b)
Resistance (GΩ)
BTEX level (ppb)
Time (min)
α-Fe2O3
RH = 0%
Topt. = 280 °C
10
15
20
25
30

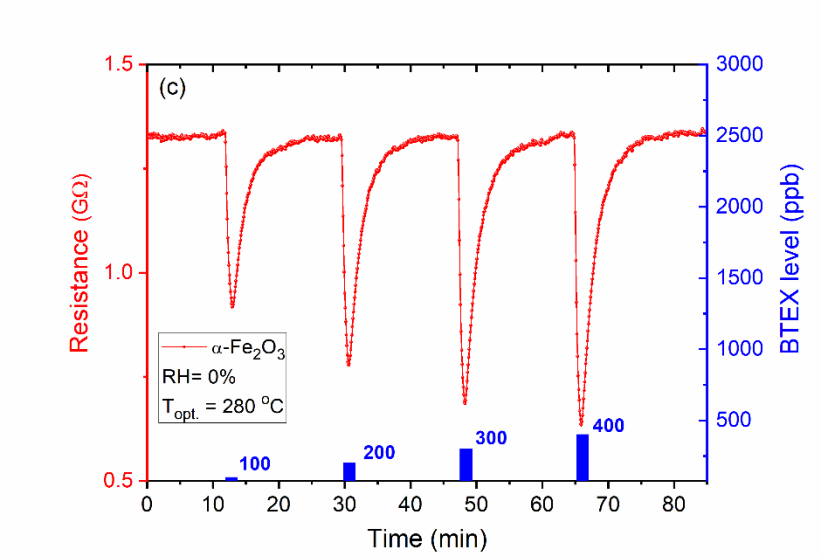
(c)
Resistance (GΩ)
BTEX level (ppb)
Time (min)
α-Fe2O3
RH= 0%
Topt. = 280 °C
100
200
300
400

Fig.6

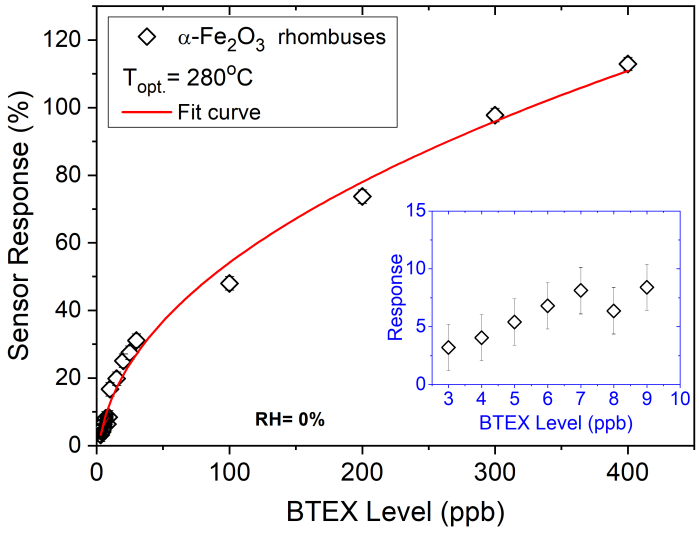
α-Fe2O3 rhombuses
Topt.= 280°C
Fit curve
RH= 0%
Sensor Response (%)
BTEX Level (ppb)
Response
BTEX Level (ppb)

Fig.7

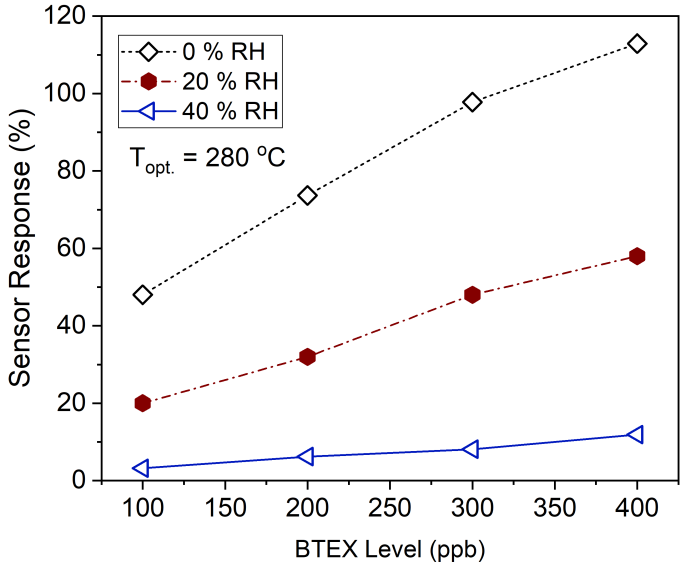
0 % RH
20 % RH
40 % RH
Topt. = 280 °C
Sensor Response (%)
BTEX Level (ppb)

Fig.8

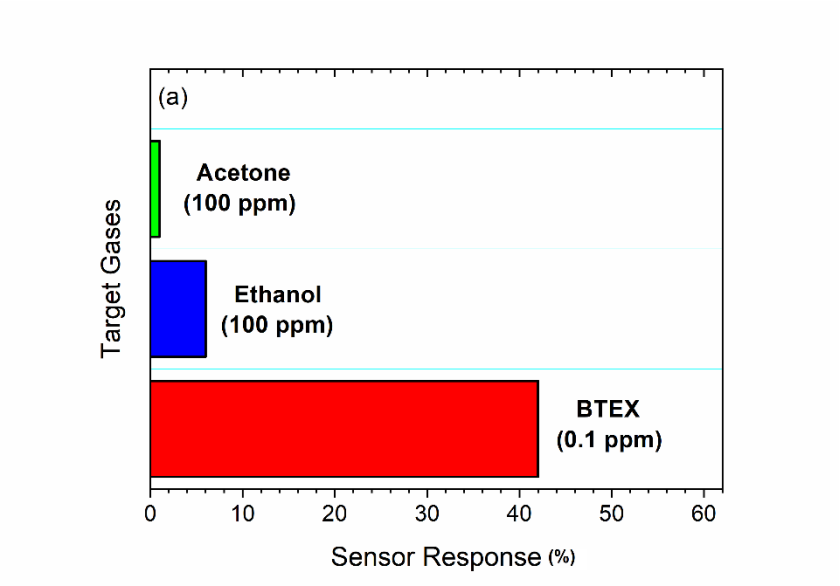
(a)
Acetone
(100 ppm)
Ethanol
(100 ppm)
BTEX
(0.1 ppm)
Target Gases
0
10
20
30
40
50
60
Sensor Response (%)

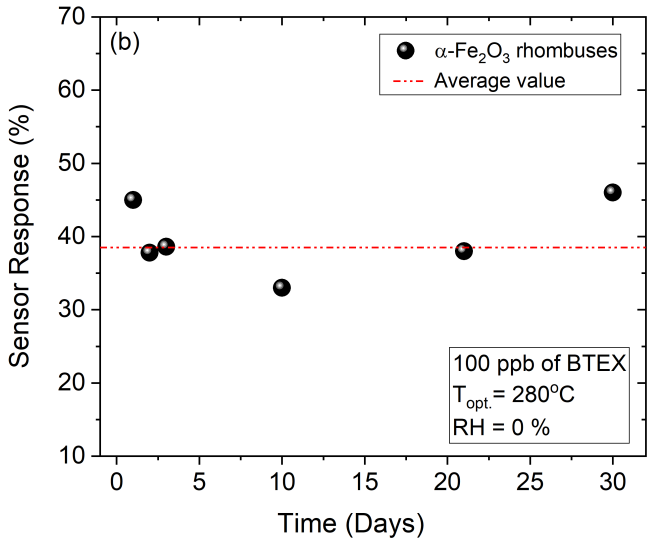
(b)
α-Fe2O3 rhombuses
Average value
100 ppb of BTEX
Topt.= 280°C
RH = 0 %
Sensor Response (%)
70
60
50
40
30
20
10
0
5
10
15
20
25
30
Time (Days)

Fig.9

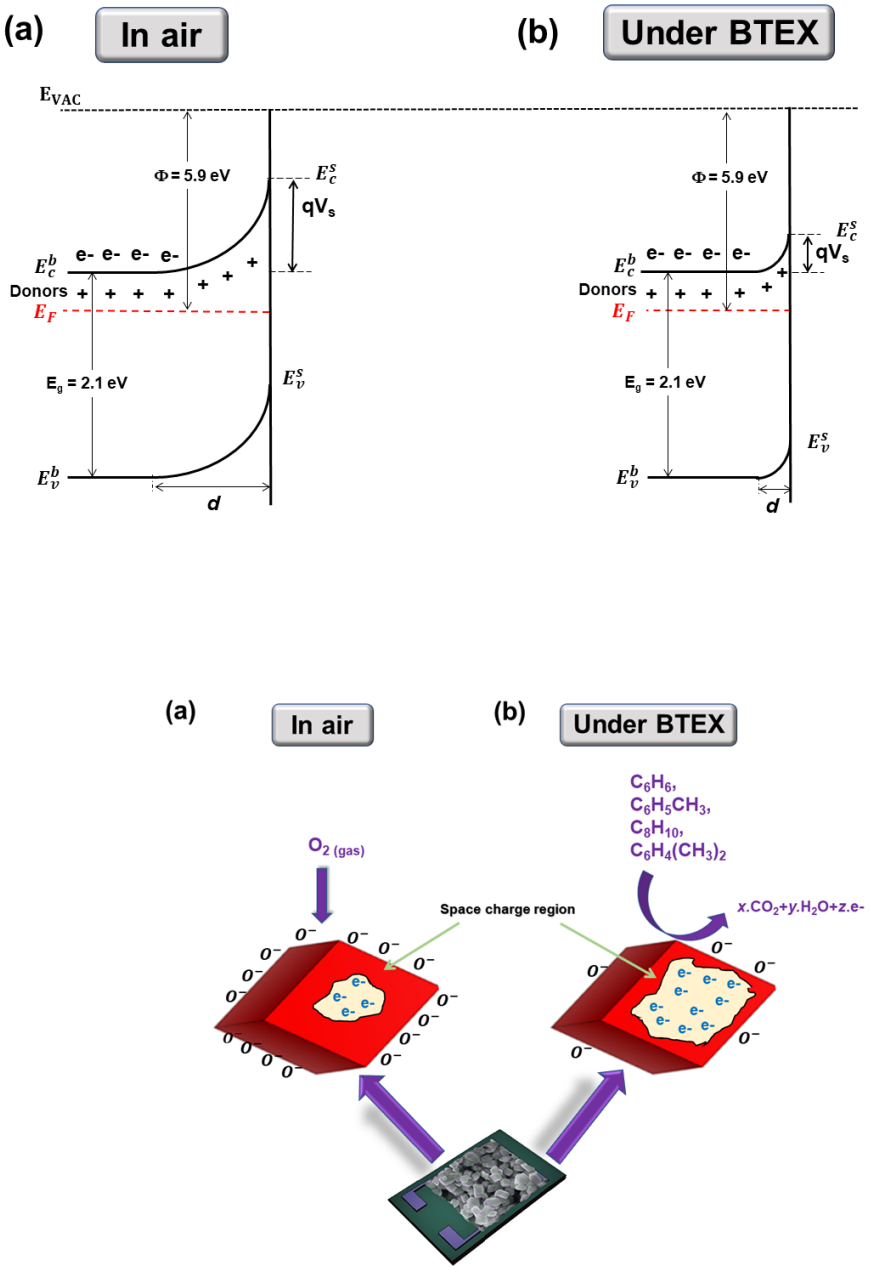
(a)
In air
(b)
Under BTEX
E_{VAC}
Φ = 5.9 eV
E_c^s
qV_s
E_c^b
e- e- e- e-
Donors + + + + + + +
E_F
E_g = 2.1 eV
E_v^s
E_v^b
d
O_2 (gas)
C_6H_6,
$C_6H_5CH_3$,
C_8H_{10},
$C_6H_4(CH_3)_2$
Space charge region
$x.CO_2+y.H_2O+z.e^-$
O⁻